

Article

# The Effect of Quenching and Partitioning (Q&P) Heat Treatment on the Microstructure and Mechanical Properties of High Boron Steel

Zhao Li <sup>1</sup>, Run Wu <sup>1,\*</sup>, Mingwei Li <sup>1</sup>, Song-Sheng Zeng <sup>2</sup>, Yu Wang <sup>3</sup> , Tian Xie <sup>1</sup> and Teng Wu <sup>1</sup>

<sup>1</sup> Key Laboratory for Ferrous Metallurgy and Resources Utilization of Ministry of Education, Wuhan University of Science and Technology, Wuhan 430081, China; lizhaodoc@hotmail.com (Z.L.); li1725217198@163.com (M.L.); xt\_zoe@163.com (T.X.); wuteng@wust.edu.cn (T.W.)

<sup>2</sup> Valin ArcelorMittal Automotive Steel Co., Ltd., Loudi 417009, China; zsscsu@sina.com

<sup>3</sup> Mark Wainwright Analytical Centre, University of New South Wales, Sydney, NSW 2052, Australia; yu.wang@unsw.edu.au

\* Correspondence: runwu@wust.edu.cn

**Abstract:** High boron steel is prone to brittle failure due to the boride distributed in it with net-like or fishbone morphology, which limit its applications. The Quenching and Partitioning (Q&P) heat treatment is a promising process to produce martensitic steel with excellent mechanical properties, especially high toughness by increasing the volume fraction of retained austenite (RA) in the martensitic matrix. In this work, the Q&P heat treatment is used to improve the inherent defect of insufficient toughness of high boron steel, and the effect mechanism of this process on microstructure transformation and the change of mechanical properties of the steel has also been investigated. The high boron steel as-casted is composed of martensite, retained austenite (RA) and eutectic borides. A proper quenching and partitioning heat treatment leads to a significant change of the microstructure and mechanical properties of the steel. The net-like and fishbone-like boride is partially broken and spheroidized. The volume fraction of RA increases from 10% in the as-cast condition to 19%, and its morphology also changes from blocky to film-like. Although the macro-hardness has slightly reduced, the toughness is significantly increased up to  $7.5 \text{ J}\cdot\text{cm}^{-2}$ , and the wear resistance is also improved.

**Keywords:** high boron steel; Q&P heat treatment; retained austenite; TRIP effect; wear resistance



**Citation:** Li, Z.; Wu, R.; Li, M.; Zeng, S.-S.; Wang, Y.; Xie, T.; Wu, T. The Effect of Quenching and Partitioning (Q&P) Heat Treatment on the Microstructure and Mechanical Properties of High Boron Steel. *Materials* **2021**, *14*, 1556. <https://doi.org/10.3390/ma14061556>

Academic Editor: Elena Pereloma

Received: 15 February 2021

Accepted: 18 March 2021

Published: 22 March 2021

**Publisher's Note:** MDPI stays neutral with regard to jurisdictional claims in published maps and institutional affiliations.



**Copyright:** © 2021 by the authors. Licensee MDPI, Basel, Switzerland. This article is an open access article distributed under the terms and conditions of the Creative Commons Attribution (CC BY) license (<https://creativecommons.org/licenses/by/4.0/>).

## 1. Introduction

In recent years, high boron steel gains many scholars' attention and has been widely used in the production of related workpieces in the fields of automotive industry, mining machinery, machine tools, etc., for its low cost [1,2], good hot workability [3–5], and high hardness. Boride (mainly  $\text{Fe}_2\text{B}$ ), as a strengthening phase in high boron steel, is superior to carbide in hardness (1450–1800 HV) and modulus of elasticity, which ensures that the steel has higher hardness and better wear resistance than white cast iron and high chromium cast iron [6,7]. However, due to the unique characteristics of boron in the microstructure, i.e., nonequilibrium boron segregation to austenite grain boundaries before quenching [8], the boride is usually distributed in net-like or fish-bone morphology in the solidified microstructure, which will seriously damage the continuation of the matrix, resulting in the inherent defect of insufficient toughness in high boron steel. Furthermore,  $\text{Fe}_2\text{B}$  exhibits serious brittleness because of the weak B–B bond along [2] crystal orientation [9–13], which will make it easily peeled off during the wear process and deteriorate the wear resistance of the steel [14]. These extremely limit the application of high boron steel on the impacting condition.

Alloying and high-temperature heat treatment are effective ways to improve the toughness of high boron steel. The Fe<sub>2</sub>B grains can be refined by Ti and Ni addition in the alloy and decomposition of net-like Fe<sub>2</sub>B is facilitated by Ce addition [15,16]. The distribution of boride is improved by modification of the alloy molten with V, Ti, and RE-Mg [17], which improves the toughness of a high boron iron-based alloy. Moreover, the addition of a small amount of Nb or Mo can help to enhance boron's hardenability in the steel, and prevent boron from forming boron carbides in the grain boundary [18–21], thereby reducing the obstructing effect of solute boron on ferrite nucleation [22]. Except for these, the net-like Fe<sub>2</sub>B can be disconnected by high temperature austenization [23,24]. Such approaches mentioned above like alloying and high temperature heat treatment are mainly focused on ameliorating the morphology of the boride, but there are few reports about improving matrix toughness. Attractive combination of strength and ductility of steel can be achieved by inserting a certain fraction of retained austenite (RA) in stronger martensite phase through Q&P heat treatment [25–27]. Therefore, Q&P heat treatment is a very novel and promising method for improving the microstructure and performance of high boron steel.

In the present study, the as-cast and Q&P heat-treated microstructures of high boron steel have been observed. In addition, the effect of Q&P heat treatment on the morphology and distribution of RA in the steel has been analyzed. Simultaneously, the macro-hardness, impact toughness, and wear resistance of high boron steel in the as-cast condition and Q&P heat-treated have been investigated. Subsequently, the wear morphologies have been observed and the wear mechanism has been discussed for the steel.

## 2. Materials and Methods

The high boron steel was fabricated by induction melting in a 50kg vacuum furnace with its chemical composition shown in Table 1. The weight fraction of boron in the steel is 1.6 wt.% to ensure the formation of the wear-resistant phase Fe<sub>2</sub>B. In order to stimulate the role of carbon and manganese in improving the toughness of the matrix during the partitioning process, the content of these two elements were set to 0.45 wt.% and 0.6 wt.%, respectively. The modifier addition of 0.5 wt.% RE-Mg was carried out in an Aluminum foil package prior to casting into metallic molds.

**Table 1.** Chemical composition of high Boron Steel/wt.%.

C	B	Mn	Al	Si	Ti	Nb	V	S	P
0.45	1.6	4.0	0.8	1.0	0.3	0.03	0.05	<0.06	<0.06

Q&P heat treatment process was realized using the combination of electric furnace and the salt baths, illustrated in Figure 1. First, the samples of the high boron steel were austenitized at 1050 °C for 2 h in the electric furnace so as to improve the morphology of eutectic borides. Subsequently, the samples were moved to the first salt bath, which was set up at the quench temperature (T<sub>q</sub>). The quenching time (t<sub>q</sub>) was set to 30 s, 60 s, 90 s, and 120 s, respectively. When the quenching temperature was reached, samples were immersed in another salt bath to realize the partitioning step (400 °C for 60 s). After partitioning the samples, water was quenched to room temperature and then final samples were obtained.

T<sub>q</sub> was set up as following: the temperature was calculated by Koistinen-Marburger equation [28]:

$$f_M = 1 - \exp[-0.011(M_s - T_q)] \quad (1)$$

Since the high boron steel contains a large volume fraction of borides, the K-M equation was appropriately changed as in Equation (2):

$$f_M = (1 - V_B)\{1 - \exp[-0.011(M_s - T_q)]\} \quad (2)$$

where  $f_M$  is the percentage of quenched martensite, and  $V_B$  is the volume fraction of boride in the structure, which is 21.3% measured by the metallo-graphical method in the as-cast microstructure in the steel. Ms point is 225 °C measured by Gleeble-3500 thermal simulation tester (DATA SCIENCES INTERNATIONAL, INC., St. Paul, MN, USA). The calculation result of  $T_q$  is shown in Figure 2. Therefore,  $T_q$  is chosen at about 160 °C.

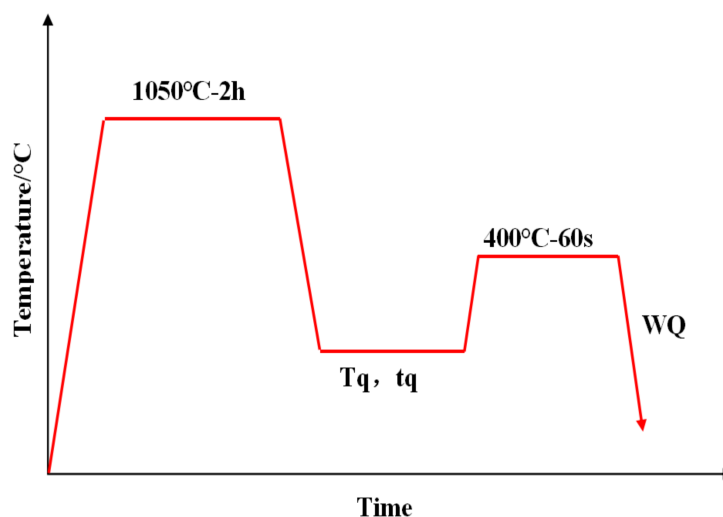


**Figure 1.** The scheme of the quenching and partitioning (Q&P) heat treatment process of the high boron steel.

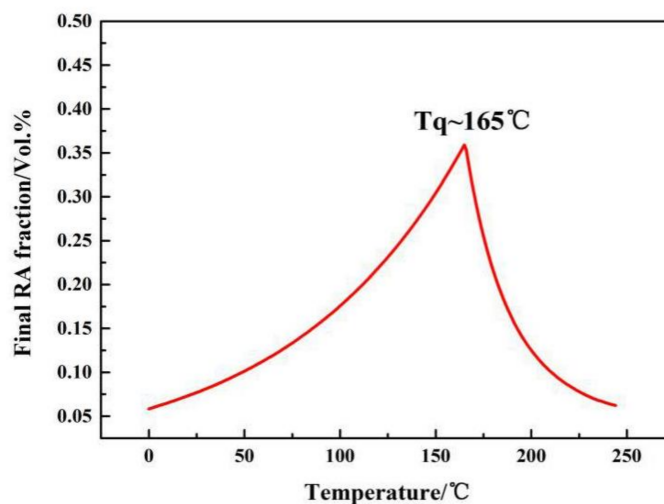


**Figure 2.** Predicted RA fraction according to Speer et al. theory.

Samples for microstructural characterization were grinded, polished, and etched in a 4% nital solution. Microstructures were observed by ZEISS metallographic microscope (Carl Zeiss AG, Oberkochen, Germany) and FEI Nova 400 Nano SEM field emission scanning electron microscope (Royal Dutch Philips Electronics Ltd., Amsterdam, Netherlands) after etching in a 4% nital solution. Transmission electron microscope (TEM), JEM-2100F (JEOL, Tokyo, Japan), was also used to characterize the microstructure of the samples, which were prepared by grinding and polishing down to a thickness of about 50  $\mu\text{m}$ , followed by double-jet thinning at  $-25$  °C with operating voltage of 32 V using 10 vol.% perchloric acid solution.

The phase composition was measured by X-ray diffraction (XRD) on a miniFlex 600 X-ray diffractometer (Lijing Scientific Instrument Co., Ltd., Shanghai, China) with  $\text{CuK}\alpha$  radiation with 40 kV and 30 mA. Samples were scanned in a  $2\theta$  range from  $40^\circ$  to  $101^\circ$  using a step size of  $0.01^\circ$ . The volume fraction of retained austenite (RA) was also measured by a LakeShore 480 magnetic measuring instrument (Linkphysics Corporation, Shanghai, China). Electron backscattering diffraction (EBSD) analysis was conducted based on the same SEM field of the samples after being vibration-polished. The data were acquired at an accelerating voltage of 20 kV, a working distance of 15 mm, a tilt angle of  $70^\circ$ , and a step size of 40 nm.

The macro-hardness of the samples was measured by an HRS-150 Rockwell hardness tester (Huayin Testing Instrument Co., Ltd., Laizhou, China) and the final value is the average of ten readings. Impact tests were performed by a JB-50 impact tester (Jianyi Experiment Equipment Co., Ltd., Wuxi, China) at room temperature. The samples had no notches with a size of  $10 \times 10 \times 55 \text{ mm}^3$  and the values reported were the averages of three tests. Dry sliding wear tests were done by the MM-2000 wear tester (Zhengli Balancing Machine Co., Ltd., Kalgan, China). The samples for the wear test with a size of  $6 \times 7 \times 15 \text{ mm}^3$ , which were cut from steel after Q&P treatment and in the as-cast condition. The GCr15 with hardness of 60–62 HRC was selected as the lower specimen and the detected samples were set as upper ones. The test parameters are an applied load of 350 N, a total time of wear being 3 h, and the speed of the lower specimen being 200 r/min. NM500 (51.3 HRC) was selected as the reference specimen. Each kind of sample and reference specimen were all subjected to three wear tests, and the mass loss were measured by the electronic balance with an accuracy of 0.1 mg. The final value is the average of three measurements, and the deviation between the maximum value and the minimum value was counted.

### 3. Results and Discussion

#### 3.1. Microstructural Characterization

##### 3.1.1. Microstructure of High Boron Steel in the As-Cast Condition

Figure 3 exhibits the optical and scanning electron micrographs of the high boron steel in the as-cast condition. From Figure 3a,b, it can be seen that the high boron steel is composed of matrix and a eutectic microstructure. According to the XRD spectrum (Figure 4), it is evident that the phases of the high boron steel are  $\alpha\text{-Fe}$ ,  $\gamma\text{-Fe}$ ,  $\text{M}_2\text{B}$ , and  $\text{M}_{23}(\text{B,C})_6$ , where M represents Fe or Mn and  $\gamma\text{-Fe}$  phase indicates the existence of retained austenite (RA) in the microstructure. Martensite is identified as  $\alpha\text{-Fe}$ . Furthermore, the borides in eutectic show net-like and rod-like morphology.

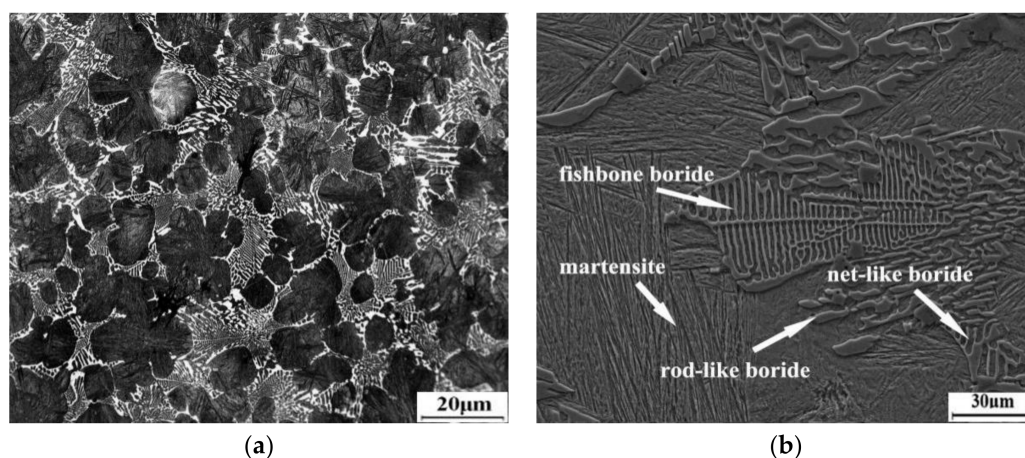


**Figure 3.** As-cast microstructure of experimental steel: (a) OM micrography and (b) SEM micrography.

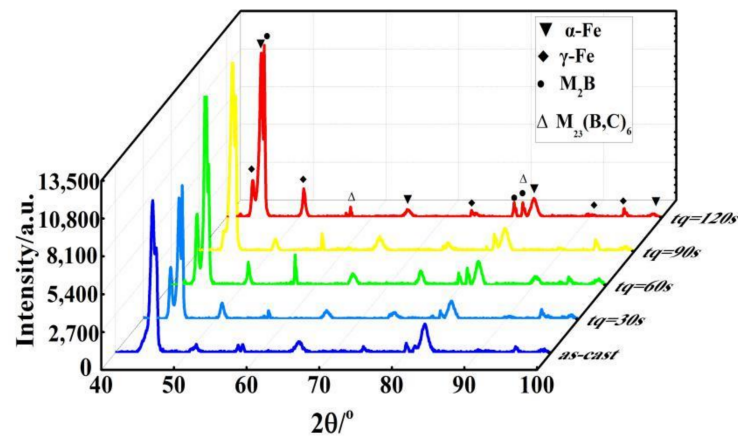


**Figure 4.** X-ray diffraction (XRD) spectra of samples in the as-cast condition and under different tq.

The microstructure resulted from the solidification of the high boron steel. The boron concentration of the remaining melt increases with the formation of dendrites due to the low solubility of boron in austenite, resulting in the formation of various eutectic borides around the dendrites. First,  $\gamma$  proeutectic transformation occurs as the liquid is cooled below the liquidus temperature. The  $\gamma$  grows in a form of dendrite and exclude boron atoms in liquid. When B-enriched molten steel reaches a eutectic point, eutectic reaction occurs:  $L \rightarrow \gamma + \text{Fe}_2\text{B}$ . In addition, a very small amount of secondary boron carbide,  $\text{M}_{23}(\text{B,C})_6$ , precipitates from the matrix during the cooling process. The formation of boride requires a large number of alloying elements. There is a strong p-d interaction between B and Fe, Mn atoms as two adjacent elements, which will form strong covalent bonds of Fe-B and Mn-B. Therefore, Mn will displace part of Fe and increase Mn content in borides around dendrites. After solidification, martensite transformation will occur in the austenite, and, finally, the matrix is composited of martensite laths and RA shown in Figure 3b.

### 3.1.2. Microstructure of High Boron Steel after Q&P Heat Treatment

After being treated by the Q&P process, the phase composition of the steel is the same as that of as-cast condition, but the intensity of the austenite peak is significantly increased in the XRD diffraction pattern of the samples from tq 30 s to 120 s, as shown in Figure 4. However, the microstructures are clearly different. The microstructures of the high boron steel after Q&P heat treatment are shown in Figure 5, where Figure 5a,c,e,g are optical microstructures and Figure 5b,d,f,h are SEM microstructures.

The boride in eutectic is partially spheroidized and fractured in all the samples after austenitizing ( $1050\text{ }^\circ\text{C} + 2\text{ h}$ ). During solidification, the necking and weak joints occur in the boride branches by the influence of the modifier. By analysis of thermodynamics, the interface energy between necking and weak joints of the boride and matrix is larger than that between spherical boride and the matrix [17,29]. In the austenization process, the difference of the interface energy result is the morphology of the boride, which is partially changed to fracture-like and spheroid-like from net-like. The matrix microstructure in the dendrite is observed to be un-tempered martensite (UM) and tempered martensite (TM). In the sample's quenched time (tq) of 30 s, a gray white structure is observed, which show lath martensite as seen in Figure 5a,b, called UM. In the one with tq for 60 s, a black structure with clear lath is observed in the matrix, which is called TM (Figure 5c,d).

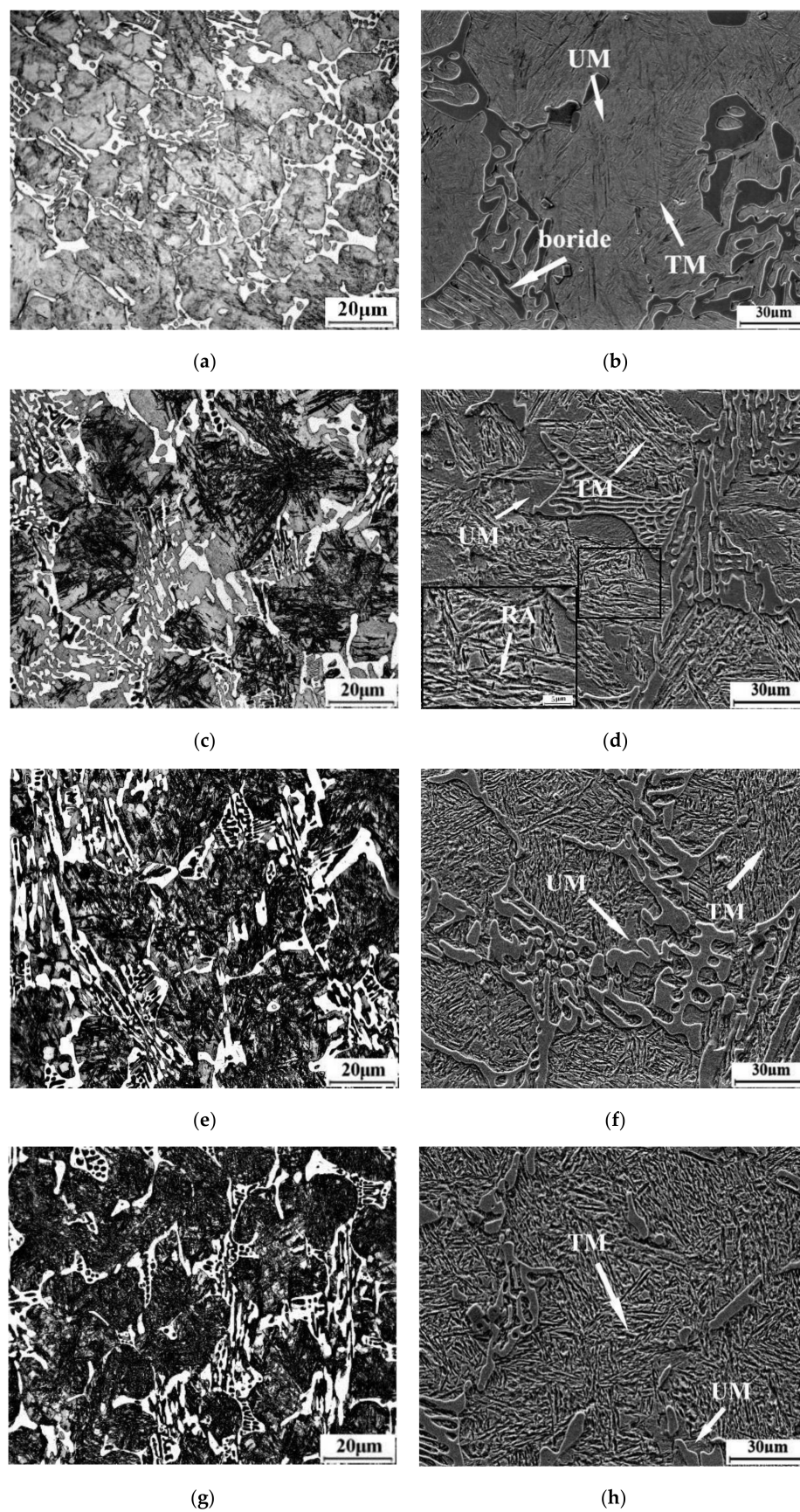


Figure 5. The microstructure of samples under different  $t_q$ : (a,b)  $t_q = 30$  s, (c,d)  $t_q = 60$  s, (e,f)  $t_q = 90$  s, (g,h)  $t_q = 120$  s.

Figure 6 exhibits the quantitative results of samples' microstructure after Q&P heat treatment. The boride decreased slightly from 21.3% of the as-cast condition to approximately 18%, and remain nearly the same amount in the partitioning with the extension of  $t_q$  due to  $M_2B$  that will not change in the subsequent partitioning process, and the change of the matrix in the eutectic is consistent with that of the matrix structure of austenite dendrite. However, the volume fraction of TM gradually increases, which are 4% ( $t_q = 30$  s), 36% ( $t_q = 60$  s), and 57% ( $t_q = 90$  s) to 67% ( $t_q = 120$  s), respectively. Meanwhile, the volume fraction of UM gradually decreases with the volume fraction of 79% ( $t_q = 30$  s), 46% ( $t_q = 60$  s), 27% ( $t_q = 90$  s) to 15% ( $t_q = 120$  s).

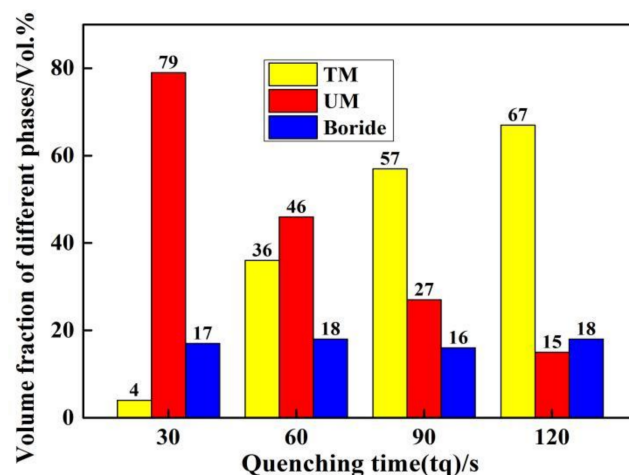


Figure 6. Quantitative results of samples under different  $t_q$ .

The microstructure quenched from austenizing is detected to have transformation during the partitioning process. The carbon atoms are diffused from the martensite into RA, which improves its thermostability. Meanwhile, the carbides precipitates within the martensite, and a tempered martensite is finally obtained with the name of TM. The UM is the product of the martensitic transformation of RA. In the partitioning process, some of RA cannot be obtained as sufficient carbon to enhance its thermostability. This part of RA is transformed into martensite when the samples are cooled down to room temperature. The new formed martensite, called UM, show a gray-white microstructure.

The volume fraction of RA in the sample changes after Q&P heat treatment. It can be observed from Figure 7 that the fraction of RA increases from 4.2% to 19.7% as the  $t_q$  increases. It is noted that the fraction of RA decreases from 10% in the as-cast condition to 4.3% when  $t_q$  is 30 s. This is because the short  $t_q$  results in a small volume fraction of martensite formed in the microstructure after quenching from austenizing, so that only a very small amount of carbon can be diffused into the RA during the subsequent partitioning at a temperature of 400 °C for 60 s. Therefore, only a small fraction of RA can be stabilized to room temperature. However, with the extension of  $t_q$ , the martensite fraction in the microstructure increased after quenching, so that more carbon can be diffused into the RA during the partitioning process, which improved the stability of RA.

### 3.2. Distribution and Morphology of Retained Austenite in the High Boron Steel before and after Q&P Heat Treatment

The distribution of RA is characterized by EBSD, as shown in Figure 8. In the EBSD phase maps,  $Fe_2B$  phase is blue, the RA phase is red, and the martensite phase is gray. The amount of RA is increased between the eutectic borides and in the dendrite by quenching from 60 s to 120 s. It is attributable to the increase of martensite content in the samples after quenching from austenizing, and, therefore, more carbon atoms can be diffused from the martensite to the adjacent austenite crystals in partitioning. The thermostability of RA is, therefore, enhanced by the increase of carbon content, which results in more RA stabilized

at room temperature. Additionally, the more RA is observed in the matrix (Figure 8a,c) near to borides and especially in the eutectic microstructure (Figure 8b,d), making more uniform distribution of RA.

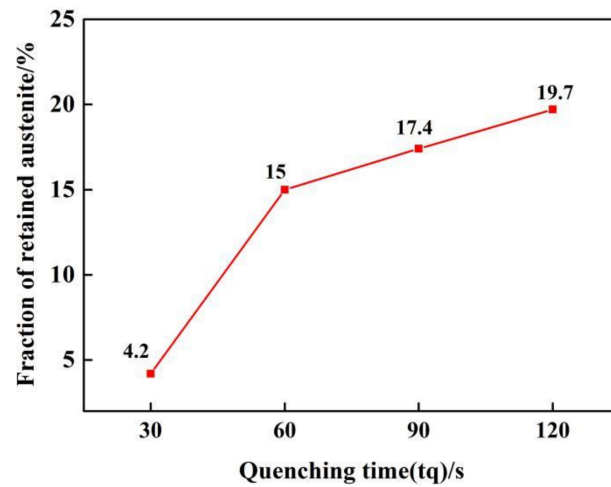


Figure 7. Changes in fraction of RA in the microstructure under different tq.

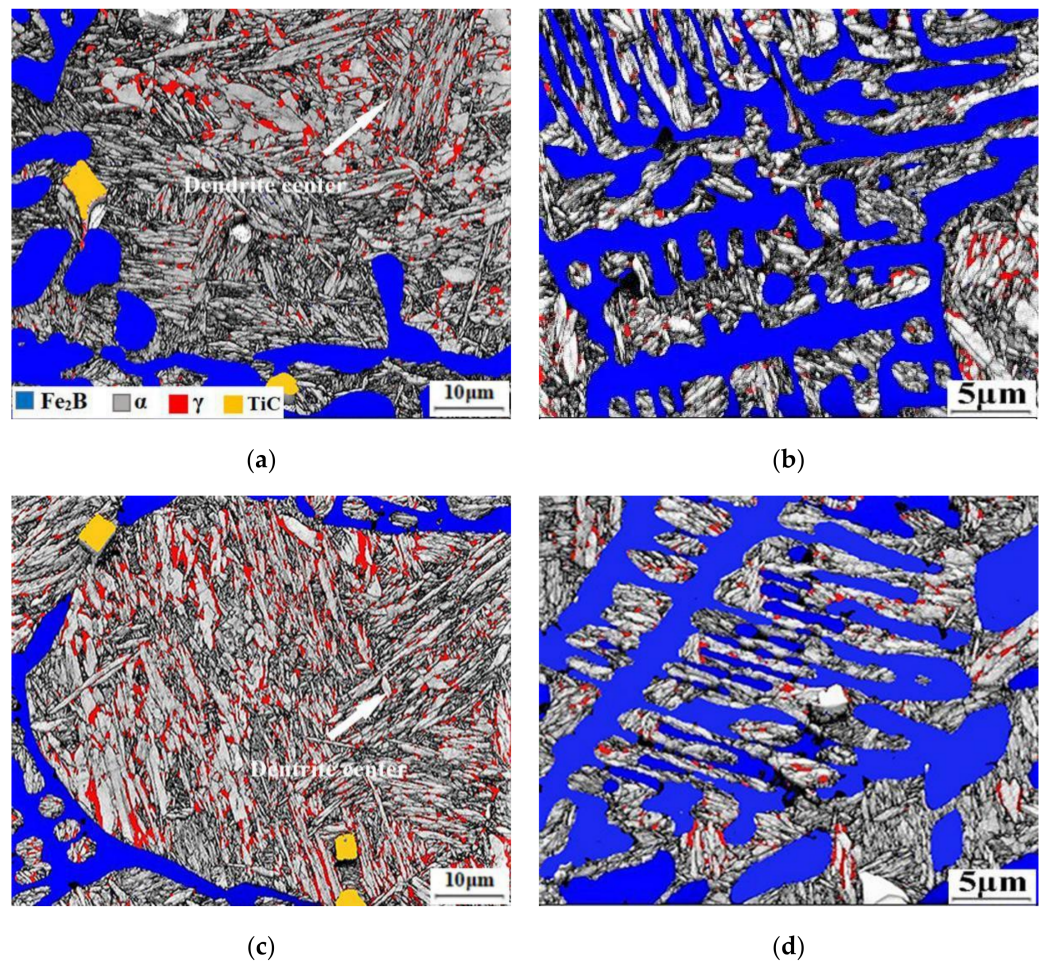
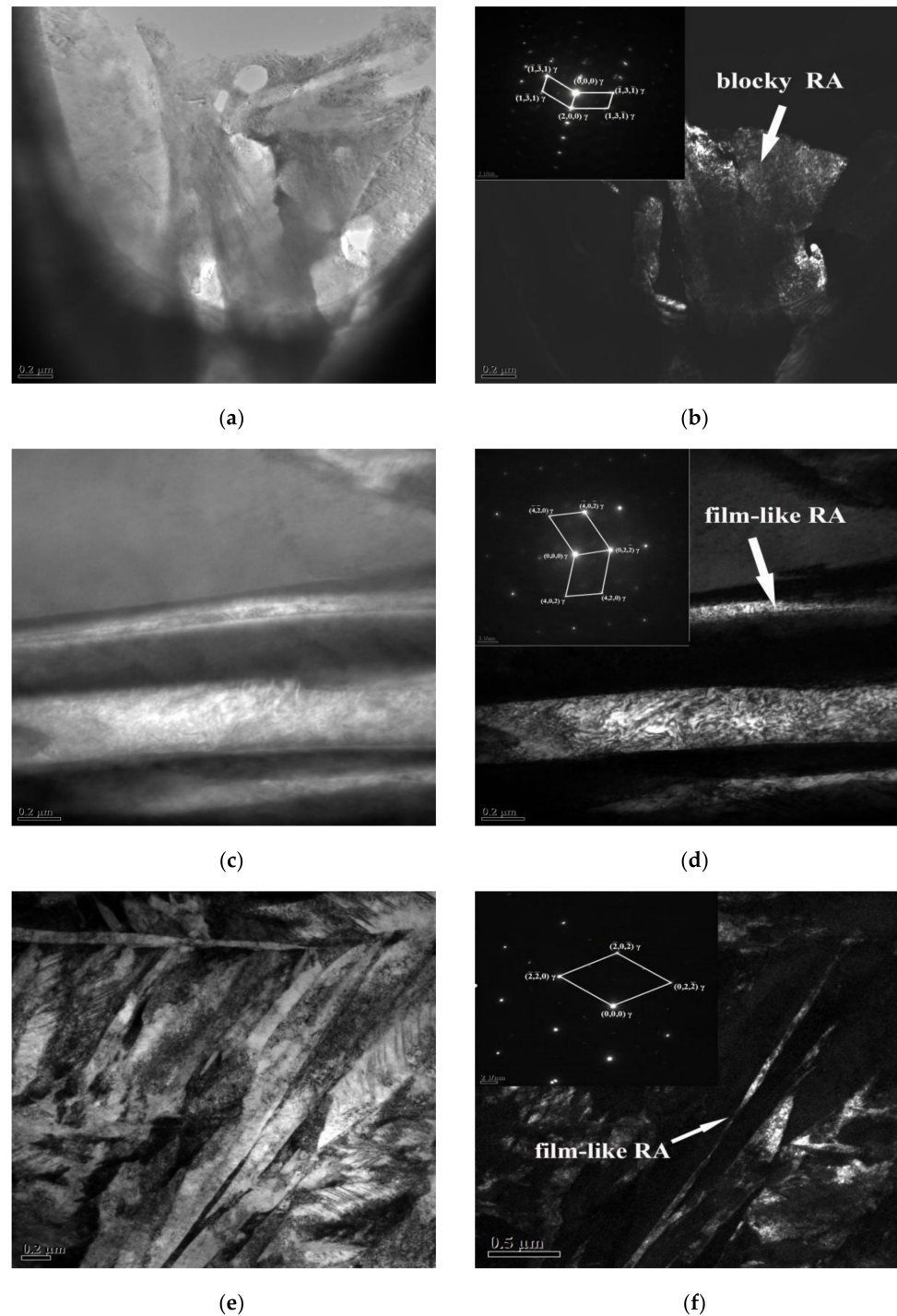


Figure 8. EBSD phase map analysis results of samples: (a,b) tq = 60 s, (c,d) tq = 120 s.

Difference of RA morphology is detected in the as-cast sample and in the Q&P treated ones by TEM, as shown in Figure 9. The blocky RA is observed in the eutectic microstructure of as-cast samples from Figure 9a,b, with a width of about 0.7  $\mu\text{m}$ . However, after Q&P

heat treatment, film-like RA in the width of about 30 nm appears between martensite laths in the samples with  $t_q$  of 90 s and 120 s. The reasons are as following. The segregation of Mn and C in the as-cast microstructure during solidification, causing RA to exist in block morphology at the edge of the dendrite. The composition of the samples is homogenized by high-temperature austenitization in Q&P heat treatment, and the martensite can uniformly nucleate in the matrix, resulting in the formation of film-like RA between martensite laths. RA presenting film-like has better transformation stability compared with a blocky type, which tends to transform to martensite under a small stress and contributes little to the TRIP effect [30–33] and can hardly improve the mechanical properties of the steel.



**Figure 9.** The TEM morphology of samples: (a,b) as-cast, (c,d)  $t_q = 90$  s, and (e,f)  $t_q = 120$  s.

### 3.3. Effect of Q&P Heat Treatment on Mechanical Properties of High Boron Steel

#### 3.3.1. Hardness and Impact Toughness of the High Boron Steel Treated by Q&P Heat Treatment

Table 2 lists hardness and impact toughness of samples treated at different tq. The hardness of the samples gradually decrease from 61.8 to 55.3 HRC with tq increases from 30 s to 120 s. Only the hardness of the sample treated at tq of 30 s is 61.8 HRC, which is higher than that of the as-cast condition (59.0 HRC). The hardness increase is due to the homogenization of composition and elimination of blocky RA after Q&P treatment. However, the decrease in hardness is the result of the increase of the soft phase RA in the microstructure with the extension of the tq.

**Table 2.** The hardness and impact toughness of samples treated at different tq.

tq/s	Hardness/HRC	Impact Toughness/J·cm <sup>-2</sup>
30	61.8	4.4
60	58.0	5.6
90	56.1	7.5
120	55.3	6.3

The impact toughness of high boron steel is improved by Q&P heat treatment. Compared with the as-cast sample (3.7 J·cm<sup>-2</sup>), the toughness of samples treated at different tq all gets improved and reaches the maximum (7.5 J·cm<sup>-2</sup>) in the sample with tq of 90 s. Figure 10 shows the impact fracture surface of samples. It can be seen from Figure 10a that the dendrite zone is quasi-cleavage fracture, while there are clear boride pits in the eutectic zone, which are mostly left by intergranular fractures along the interface between the boride and the matrix. When tq is 90 s, as shown in Figure 10b, the dendritic zone is filled with dimples and fishbone boride is covered by the ductile matrix in the eutectic zone. The improvement of toughness is attributed both to the fracture or spheroidization of the boride and also to the increase of matrix toughness [34,35]. For high boron steel, cracks will occur and propagate at the interface between boride and matrix during impact. The appearance of film-like RA between the martensite laths will help improve the toughness of the matrix and delay the cracking of the interface.

However, as tq increased to 120 s, it can be seen from Figure 10c that the same dimples exist in the dendritic region, but the eutectic region is composed of a large number of smooth regions, which is different from Figure 9b. In addition, the impact toughness decreases to 6.3 J·cm<sup>-2</sup>. This is related to the hardness decrease of the matrix, which is caused by an excessively high fraction of RA (19.4%) in it, which leads to the partial boride that can hardly be supported by the matrix. Therefore, boride will fall off from the interface, resulting in a large number of brittle fractures in the eutectic region.

#### 3.3.2. Effect of tq on the Wear Property of High Boron Steel

Q&P heat treatment is beneficial for the improvement of the wear resistance of high boron steel. Mass loss records and measurement deviations after a dry sliding wear test are plotted in Figure 11. The deviation of mass loss of different samples and reference specimens (NM500) fluctuates between 0.001 or 0.002 g, which proves the validity of the measurement data. After sliding for 3 h, the mass loss of the as-cast sample is 0.084 g, which is lower than NM500 (0.124 g). The mass loss of samples after Q&P heat treatment are 0.06 g (tq = 30 s), 0.067 g (tq = 60 s), 0.065 g (tq = 90 s), and 0.075 g (tq = 120 s), and that of all the samples are below that of the as-cast sample.

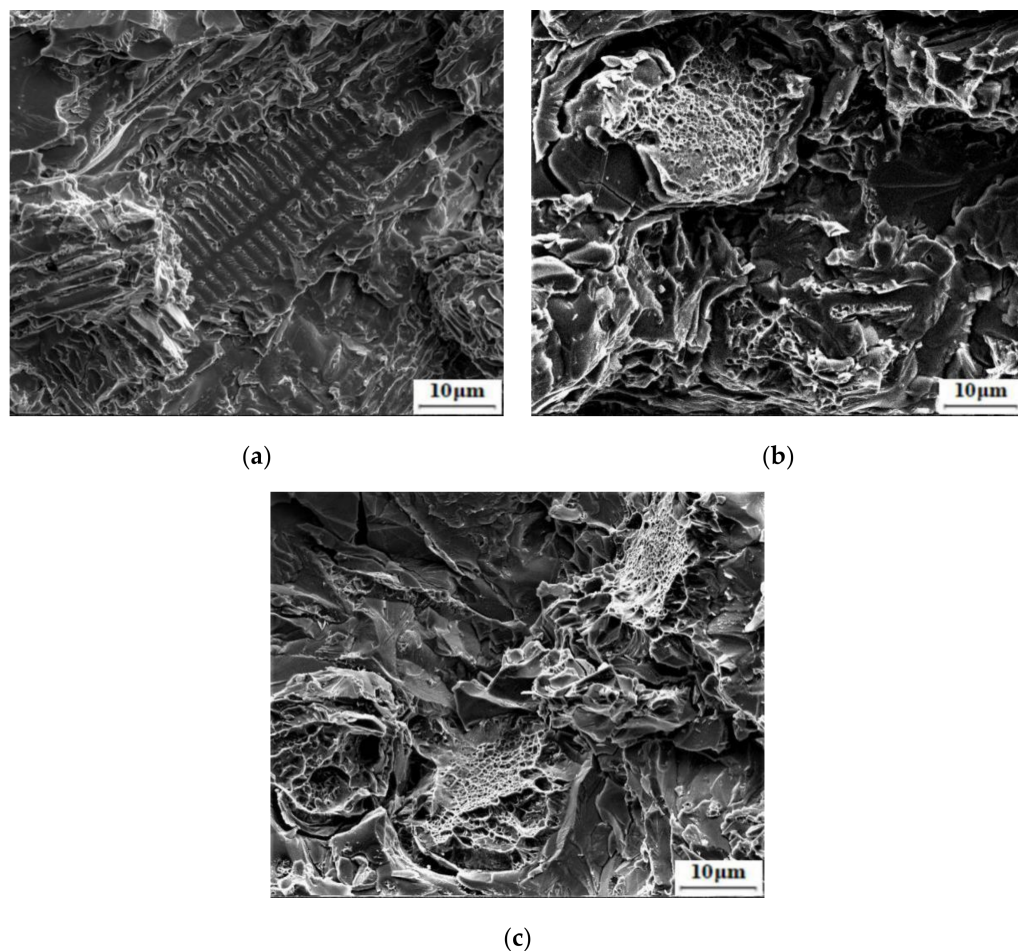


Figure 10. SEM fractographs of samples: (a) as-cast, (b) tq = 90 s, and (c) tq = 120 s.

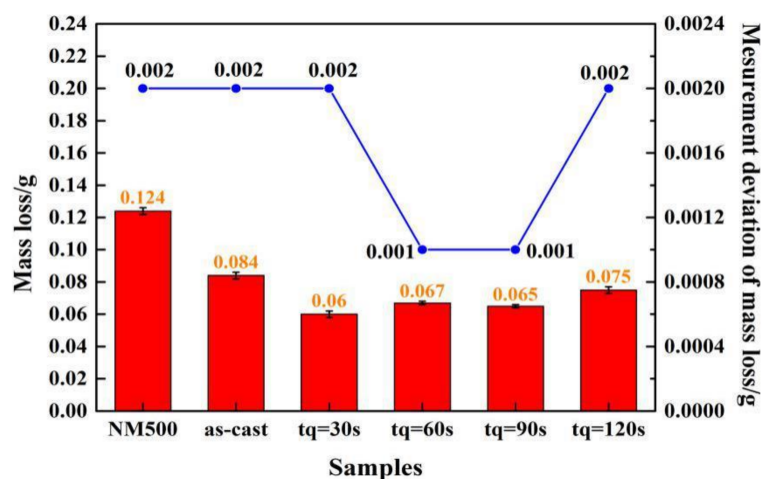
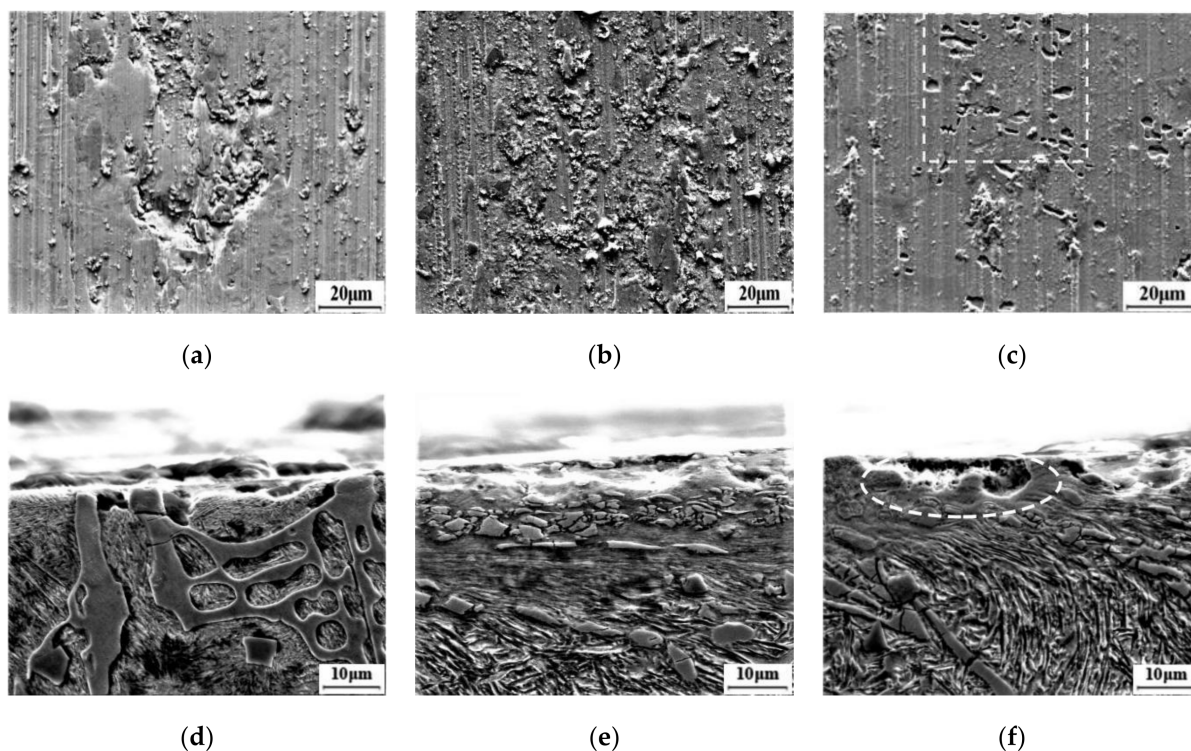


Figure 11. Mass loss and measurement deviation of samples and a reference specimen.

The wear resistance of high boron steel is affected by the matrix microstructure. The sample with tq of 30 s shows better wear resistance due to the higher hardness of the matrix. However, as the tq increases, the fraction of RA in the microstructure gradually increases to make the hardness of the matrix decrease. The decrease of the matrix hardness causes a larger wear loss. Besides, the mass loss of the sample with tq of 90 s is lower than that of the sample with 60 s, which is likely due to the martensitic transformation from film-like RA caused by the wear stress in the surface layer.

The transformation during the wear process can be demonstrated by Figure 12. In the as-cast sample, the brittle spalling pits and grooves along the sliding direction are observed on the worn surface, shown in Figure 12a. It can be seen from Figure 12d that the coarse borides are broken in the worn subsurface on the section microstructure. Jian et al. [36] demonstrated that  $\text{Fe}_2\text{B}$  can hardly be deformed due to its high hardness and elastic modulus but will cause brittle spalling from the matrix during the wear process. Few pits and grooves are observed on the worn surface of the samples with  $t_q$  of 90 s, as shown in Figure 12b, and a thicker deformation zone is observed in the section microstructure (Figure 12e). Although they are broken, the borides are deformed along the sliding direction, making the clear flow lines appear in the deformation zone.



**Figure 12.** Worn surfaces and sub-surfaces morphology of samples: (a,d) as-cast, (b,e)  $t_q = 90$  s, and (c,f)  $t_q = 120$  s.

The worn surface of the sample is affected by both the compressive stress from the load and the shear stress of the lower specimen during the wear process. Berkowski et al. [37] demonstrated that carbide microcracks are the center of fracture nucleation as well as fatigue spalling in ledeburitic chromium steels. For the as-casted high boron steel, the boride is coarse and concentrated with clear microcracks, and has a long and unstable interface with the matrix, as shown in Figure 12d, which will cause brittle spalling of the martensite matrix under the shear stress from the lower specimen. The boride without support from matrix will be exposed on the worn surface, and will be gradually broken and peeled off under the compressive stress and shearing stress, resulting in a large amount of mass loss. A thicker deformation zone is observed in the worn subsurface layer of the sample with  $t_q$  of 90 s (Figure 12e), in which there are clear flow lines and doped with many boride particles. RA will induce martensite nucleation under plastic deformation, and the phase transformation strengthening (TRIP effect) will increase the toughness of the matrix to better support the boride particles. In addition, many non-shedding oxidized wear adhesive particles are produced on the worn surface during the wear process (Figure 12b), which will hinder the wear process and improve wear resistance of the steel. It is comparable to the results of Kazimierz et al. [38] on the tribological behavior that AlCrSiN-Coated Tool Steel K340, that is, a large number of relatively large carbides constitute a natural obstacle to the counter body material, and the adhesive wear

makes the wear rate of the sample lower than the abrasive wear, as demonstrated in the literature [39].

However, RA in an excessive amount is not beneficial to the wear resistance of the high boron steel. The peeling pits appeared on the worn surface since the sample with  $t_q$  of 120 s contains 19.7 wt.% of RA, as shown in the dashed box in Figure 12c. A few deformed flow lines and spalled pits are observed within a thinner deformation zone on its section microstructure (the dashed box in Figure 12f). During the wear process, RA in the surface layer is worn off because of its low hardness before it transforms to martensite. Then, the matrix can hardly support the broken borides effectively. Therefore, it increases the mass loss of the sample.

#### 4. Conclusions

The usual toughening methods for high boron steel, such as alloying and high temperature heat treatment, mostly focus on the improvement of boride morphology, but have a very limited effect on enhancing the toughness of the matrix. Inspired by the production of Q&P steel, Q&P heat treatment was used for high boron steel in this work. The results show that microstructural and mechanical properties, especially toughness and wear resistance of the steel, have been improved successfully after being treated because this process can only ensure the improvement of boride morphology by austenitization. However, the process also enables more fraction RA in the matrix that can be stabilized to room temperature through the steps of quenching and partitioning. It will provide guidance for production and the optimization of a heat treatment process of high boron steel.

The insights regarding the present study have been obtained as the following.

- (1) The microstructure of as-cast high boron steel is composed of pro-eutectic austenite dendrites and eutectic, which is from the reaction of  $L \rightarrow \gamma + Fe_2B$ . After solidification, the transformation will occur in the austenite. The borides in eutectic show net-like and rod-like morphology without change in cast cooling and, finally, the matrix is composited of martensite laths and RA.
- (2) After being treated by the Q&P process, the borides are partially broken and spheroidized successfully. The matrix is composed of UM and TM and the morphology of RA is mostly changed from blocky to film-like. As the  $t_q$  in the Q&P process extend from 30 s to 120 s, the volume fraction of RA in the microstructure increases from 4.2% to 19.7% and the distribution becomes more uniform.
- (3) Although the macro-hardness of the samples gradually decreases from 61.8 to 55.3 HRC with the extension of  $t_q$ , the toughness is significantly improved, compared with the as-cast sample, and reaches the maximum ( $7.5 \text{ J}\cdot\text{cm}^{-2}$ ) when  $t_q$  is 90 s. In a dry sliding test, the mass loss of treated samples are about 0.06–0.075 g, which shows better wear resistance than that of the as-cast sample (0.084 g) and NM500 (0.124 g).
- (4) Mechanical properties improvement is attributable to the change of boride morphology and the improvement of the matrix by increasing the volume fraction of RA. However, as a soft phase in steel, excessive volume fraction of RA will inevitably lead to a decrease in the hardness of the matrix, resulting in deterioration of toughness and wear resistance. From the experimental results of the high boron steel, the volume fraction of RA should be controlled at about 16%.

**Author Contributions:** Z.L. carried out the experiments, wrote, and edited the manuscript. R.W. supervised the results, analyzed the data, and wrote the manuscript. M.L., S.-S.Z., Y.W., and T.X. contributed to the interpretation of the data and edited the manuscript. T.W. analyzed the data and managed the project. All authors have read and agreed to the published version of the manuscript.

**Funding:** This research project is financially supported by the National Natural Science Foundation of China, Beijing, China (Grant no. 51771139).

**Institutional Review Board Statement:** Not applicable.

**Informed Consent Statement:** Not applicable.

**Data Availability Statement:** Not applicable.

**Acknowledgments:** The authors would like to acknowledge the National Natural Science Foundation of China for funding this project.

**Conflicts of Interest:** The authors declare no conflict of interest.

## References

1. Lentz, J.; Röttger, A.; Theisen, W. Solidification and Phase Formation of Alloys in the Hypoeutectic Region of the Fe–C–B System. *Acta Mater.* **2015**, *99*, 119–129. [[CrossRef](#)]
2. Ma, S.; Xing, J.; Liu, G.; Yi, D.; Fu, H.; Zhang, J.; Li, Y. Effect of Chromium Concentration on Microstructure and Properties of Fe–3.5B alloy. *Mater. Sci. Eng. A* **2010**, *527*, 6800–6808. [[CrossRef](#)]
3. Cao, B.; Wang, X.M.; Cui, H.Y.; He, X.L. Non-Equilibrium Segregation of Boron on Grain Boundary in Fe-30%Ni alloy. *Int. J. Min. Met. Mater.* **2002**, *9*, 347–351.
4. Irati, Z.; Nerea, I.; Eric, D.; Volker, S.; Hardy, M.; Pello, U. Toughness Property Control by Nb and Mo Additions in High-Strength Quenched and Tempered Boron Steels. *Metals* **2021**, *11*, 95. [[CrossRef](#)]
5. Jahazi, M.; Jonas, J. The Non-Equilibrium Segregation of Boron on Original and Moving Austenite Grain Boundaries. *Mater. Sci. Eng. A* **2002**, *335*, 49–61. [[CrossRef](#)]
6. Ozdemir, O.; Usta, M.; Bindal, C.; Ucisik, A. Hard Iron Boride (Fe<sub>2</sub>B) on 99.97wt% Pure Iron. *Vacuum* **2006**, *80*, 1391–1395. [[CrossRef](#)]
7. Berns, H.; Saltykova, A.; Röttger, A.; Heger, D. Wear Protection by Fe-B-C Hard Phases. *Steel Res. Int.* **2011**, *82*, 786–794. [[CrossRef](#)]
8. Irati, Z.; Nerea, I.; Eric, D.; Volker, S.; Hardy, M.; Pello, U. Effect of Nb and Mo Additions in the Microstructure/Tensile Property Relationship in High Strength Quenched and Tempered Boron Steels. *Metals* **2021**, *11*, 29. [[CrossRef](#)]
9. Ma, S.; Xing, J.; He, Y.; Fu, H.; Li, Y.; Liu, G. Effect of Orientation and Lamellar Spacing of Fe<sub>2</sub>B on Interfaces and Corrosion Behavior of Fe-B Alloy in Hot-Dip Galvanization. *Acta Mater.* **2016**, *115*, 392–402. [[CrossRef](#)]
10. Jian, Y.; Huang, Z.; Xing, J.; Wang, B. Effects of Chromium Addition on Fracture Toughness and Hardness of Oriented Bulk Fe<sub>2</sub>B Crystals. *Mater. Charact.* **2015**, *110*, 138–144. [[CrossRef](#)]
11. Li, M.S.; Fu, X.L.; Xu, W.D.; Zhuang, R.L.; Yu, R.H. Valence Electron Structure of Fe<sub>2</sub>B Phase and its Eigen-Brittleness. *Acta Metall. Sin.* **1995**, *31*, 201–208.
12. Ücisik, A.; Bindal, C. Fracture Toughness of Boride Formed on Low-Alloy Steels. *Surf. Coat. Technol.* **1997**, *94–95*, 561–565. [[CrossRef](#)]
13. Sen, U.; Sen, S.; Koksall, S.; Yilmaz, F. Fracture Toughness of Borides Formed on Boronized Ductile Iron. *Mater. Des.* **2005**, *26*, 175–179. [[CrossRef](#)]
14. Li, K.; Huang, Z.; Jian, Y.; Min, T.; Lou, X.; Wang, S. Friction and Wear Behavior of Single-Phase Fe<sub>2</sub>B Bulk under Dry Sliding Condition. *Tribol. Trans.* **2017**, *61*, 513–521. [[CrossRef](#)]
15. Yi, D.; Xing, J.; Zhang, Z.; Fu, H.; Yang, C. Effect of Titanium and Nitrogen Additions on the Microstructures and Three-Body Abrasive Wear Behaviors of Fe–B Cast Alloys. *Tribol. Lett.* **2014**, *54*, 107–117. [[CrossRef](#)]
16. Yi, D.; Zhang, Z.; Fu, H.; Yang, C.; Ma, S.; Li, Y. A Study on the Microstructures and Toughness of Fe-B Cast Alloy Containing Rare Earth. *J. Mater. Eng. Perform.* **2014**, *24*, 626–634. [[CrossRef](#)]
17. Liu, Z.-L.; Chen, X.; Li, Y.-X.; Hu, K.-H. High Boron Iron-Based Alloy and its Modification. *J. Iron Steel Res. Int.* **2009**, *16*, 37–42. [[CrossRef](#)]
18. Mohrbacher, H. Property Optimization in As-Quenched Martensitic Steel by Molybdenum and Niobium Alloying. *Metals* **2018**, *8*, 234. [[CrossRef](#)]
19. Mohrbacher, H. Synergies of Niobium and Boron Microalloying in Molybdenum Based Bainitic and Martensitic Steel. *Fundam. Appl. Mo Nb Alloy. High Perform. Steels.* **2014**, *1*, 83–108.
20. Larrañaga-Otegui, A.; Pereda, B.; Jorge-Badiola, D.; Gutiérrez, I. Austenite Static Recrystallization Kinetics in Microalloyed B Steels. *Met. Mater. Trans. A* **2016**, *47*, 3150–3164. [[CrossRef](#)]
21. Hulka, K.; Kern, A.; Schriever, U. Application of Niobium in Quenched and Tempered High-Strength Steels. *Mater. Sci. Forum* **2005**, *2005*, 519–526. [[CrossRef](#)]
22. Sharma, M.; Ortlepp, I.; Bleck, W. Boron in Heat-Treatable Steels: A Review. *Steel Res. Int.* **2019**, *90*, 1900133. [[CrossRef](#)]
23. Ma, Q.; Liu, B.C.; Wang, Z.C. Breakup of Eutectic Carbide Network of White Cast Irons at High Temperatures. *Mater. Sci.* **1995**, *30*, 3383–3386.
24. Wang, S.; Jiang, Q.; Cui, X.; He, Z. Influence of Trace Elements and Heat Treatment on Carbide Morphology and Properties of CD-2 Steel. *Mater. Sci. Eng. A* **1999**, *264*, 172–176. [[CrossRef](#)]
25. Speer, J.; Matlock, D.; De Cooman, B.; Schroth, J. Carbon Partitioning into Austenite after Martensite Transformation. *Acta Mater.* **2003**, *51*, 2611–2622. [[CrossRef](#)]
26. Varshney, A.; Sangal, S.; Kundu, S.; Mondal, K. Super Strong and Highly Ductile Low Alloy Multiphase Steels Consisting of Bainite, Ferrite and Retained Austenite. *Mater. Des.* **2016**, *95*, 75–88. [[CrossRef](#)]
27. De Moor, E.; Matlock, D.K.; Speer, J.G.; Merwin, M.J. Austenite Stabilization through Manganese Enrichment. *Scr. Mater.* **2011**, *64*, 185–188. [[CrossRef](#)]

28. Koistinen, D.; Marburger, R. A General Equation Prescribing the Extent of the Austenite-Martensite Transformation in Pure Iron-Carbon Alloys and Plain Carbon Steels. *Acta Met.* **1959**, *7*, 59–60. [[CrossRef](#)]
29. Shi, X.-L.; Jiang, Y.-H.; Zhou, R. Effects of Rare Earth, Titanium, and Magnesium Additions on Microstructures and Properties of High-boron Medium-carbon Alloy. *J. Iron Steel Res. Int.* **2016**, *23*, 1226–1233. [[CrossRef](#)]
30. Speer, J.G.; Assunção, F.C.R.; Matlock, D.K.; Edmonds, D.V. The “Quenching and Partitioning” Process: Background and Recent Progress. *Mater. Res.* **2005**, *8*, 417–423. [[CrossRef](#)]
31. De Moor, E.; Lacroix, S.; Clarke, A.; Penning, J.; Speer, J. Effect of Retained Austenite Stabilized via Quench and Partitioning on the Strain Hardening of Martensitic Steels. *Met. Mater. Trans. A* **2008**, *39*, 2586–2595. [[CrossRef](#)]
32. Xiong, X.; Chen, B.; Huang, M.; Wang, J.; Wang, L. The Effect of Morphology on the Stability of Retained Austenite in a Quenched and Partitioned Steel. *Scr. Mater.* **2013**, *68*, 321–324. [[CrossRef](#)]
33. Ding, R.; Tang, D.; Zhao, A. A Novel Design to Enhance the Amount of Retained Austenite and Mechanical Properties in Low-Alloyed Steel. *Scr. Mater.* **2014**, *88*, 21–24. [[CrossRef](#)]
34. Xiao, B.; Xing, J.; Ding, S.; Su, W. Stability, Electronic and Mechanical Properties of Fe<sub>2</sub>B. *Phys. B Condens. Matter* **2008**, *403*, 1723–1730. [[CrossRef](#)]
35. Huang, Z.; Xing, J.; Guo, C. Improving Fracture Toughness and Hardness of Fe<sub>2</sub>B in High Boron White Cast Iron by Chromium Addition. *Mater. Des.* **2010**, *31*, 3084–3089. [[CrossRef](#)]
36. Jian, Y.; Huang, Z.; Xing, J.; Sun, L.; Gao, Y.; Zheng, Q. Investigations on the Mechanical Properties and Three-Body Wear Behavior of Pure Fe<sub>2</sub>B Intermetallic with Different Chromium Additions. *Wear* **2019**, *418–419*, 273–280. [[CrossRef](#)]
37. Berkowski, L.; Borowski, J.; Rybak, Z. The Influence of Structure on the Results of the Nitriding of Ledeburitic Chromium Steels. Part VI. Ion Nitriding of NC11LV Steel Burnishing after Hardening on Martensitic Structure. *Obróbka Plast. Met.* **2009**, *20*, 3–14. (In Polish)
38. Drozd, K.; Walczak, M.; Szala, M.; Gancarczyk, K. Tribological Behavior of AlCrSiN-Coated Tool Steel K340 Versus Popular Tool Steel Grades. *Materials* **2020**, *13*, 4985. [[CrossRef](#)] [[PubMed](#)]
39. Yan, H.; Zhao, L.; Chen, Z.; Hu, X.; Yan, Z. Investigation of the Surface Properties and Wear Properties of AISI H11 Steel Treated by Auxiliary Heating Plasma Nitriding. *Coatings* **2020**, *10*, 528. [[CrossRef](#)]